Effect of Sintering Temperature on Microstructure and Strength Distribution of Alumina Coil Springs

Serkan Nohut[a*], Cláudio A. Perottoni[b], Chunsheng Lu[c], Rodrigo A. Barbieri[b], Janete E. Zorzi[b]

[a]*Faculty of Engineering, Zirve University, Kizilhisar Kampusu, Gaziantep, 27260, Turkey*

[b]*Instituto de Materiais Cerâmicos, Universidade de Caxias do Sul, 95765-000, Bom Princípio-RS, Brazil*

[c]*Department of Mechanical Engineering, Curtin University, Perth, WA 6845, Australia*

* Corresponding Author: Serkan Nohut

Tel.: +90 342 211 6789

Fax: +90 342 211 6677

E-mail address: serkan.nohut@zirve.edu.tr

Abstract

Ceramic coil springs are one of the most widely used components in mechanical systems under harsh chemical conditions and at high temperatures. In real applications of ceramic coil springs, knowing the effect of sintering temperature on their microstructure and strength distribution plays a crucial role. In this paper, the microstructure and strength distribution of alumina coil springs sintered at 1550°C, 1600°C and 1650°C are investigated. Strength data of alumina springs are fitted by the Weibull distribution and, according to the R^2 value, the deviation from the Weibull distribution is discovered. It is shown that the Weibull distribution best fits the strength data of alumina springs sintered at 1600°C. The reasons for deviation from the Weibull distribution are discussed regarding the grain size, porosity, and *R*-curve behavior.

Keywords

Alumina springs; Microstructure; Sintering temperature; Strength distribution

Introduction

The advantageous characteristics of ceramics are often offset by concerns of their high manufacturing cost and brittleness or poor toughness. To overcome these barriers and develop advanced ceramics, major progress has been achieved over the past two decades, which results in an increase of ceramic structures in various industrial areas such as electronics, information and communication, energy and environment, and mechanical engineering[1-3].

Many engineering components (e.g., bearing, wear plates, thermal plates, bushing, gears and springs) have benefited from advanced ceramics. Coil springs are nowadays produced in a wide range of materials such as chrome-silicon, high carbon steel, stainless steel, brass, zinc, and nickel alloy. However, these materials exhibit limited mechanical properties under severe service conditions. Therefore, ceramic springs are one of the most powerful candidates for applications in mechanical systems under harsh chemical and high temperature environments. In contrast to metals, ceramic springs are electrical insulators with high wear resistance, low density, good thermal resistance, and high temperature strength[4, 5]. Moreover, an important advantage of using ceramics as springs is their lower energy dissipation in each loading-unloading cycle[6, 7]. For example, ceramic springs can be used in magnetic resonance imaging scanners[8] and energy plants[9].

There are three main methods for the production of ceramic springs: machining cylindrical compacts[10], extrusion of sol-gel-derived pastes or polymer-ceramic mixtures[11] and low pressure injection molding (LPIM)[4, 5]. Among these methods, LPIM provides ceramic springs with higher surface quality and lower cost. Krindges et al.[4] developed a simple LPIM method to mold helical springs. Barbieri et al.[5] produced alumina springs under three different sintering temperatures and investigated the effect of sintering temperatures on their mechanical properties such as porosity, spring constants and the Weibull parameters.

Compared to production of ceramic springs, there are only a few studies related to their reliability[12-14]. Nohut and Schneider[12] introduced a general formulation for the prediction of failure probability of ceramic springs with various mechanical properties and dimensions. Sato et al.[13] performed compression tests with Si_3N_4 coil springs and concluded that they obey Hooke's law and maintain the high strength until 1000ºC. For a reliable use of ceramic coil springs, there is a need for the analysis of their microstructure and strength distribution in order to obtain the most suitable sintering temperature, at which springs can satisfy the required mechanical properties. The main aim of this study is to investigate the effect of sintering temperature on the strength distribution of alumina springs. The deviation of strength distributions from the Weibull distribution is explained regarding their microstructures and failure mechanisms (e.g., grain size, porosity, *R*-curve behavior etc.).

Materials & Methods

Sample and Experimental Procedure

In the production of alumina springs, commercially available submicrometer-sized alumina (Al_2O_3) A-1000SG (Almatis Inc., Leetsdale, PA) was used as received. According to the supplier's data, this 99.8% pure alumina has an average particle size of 0.4 μm. The mixture of alumina and binder for injection was prepared directly in the LPIM machine (Peltsman MIGL-33, Minneapolis, MN), with 86 wt.% of alumina and 14 wt.% of wax based binder (~55 vol.%). The mixture was mixed for 20 h at 90ºC before injection[4, 5, 15, 16].

Ceramic springs were made by a brass mold lined with a fine polytetrafluoroethylene film. The brass mold was multi-parted to simplify the mechanical extraction of green ceramic springs after injection. The alumina/binder mixture was injected into the brass mold at 90ºC and 400 kPa, keeping the pressure for 12 s. During injection, temperature of the mold was kept at 50ºC[4, 5].

The green ceramic parts were subjected to debinding immersed into an alumina powder bed (A-1000SG) up to 250ºC[4, 5]. Then, the parts were fired to 1000ºC in an electrical resistance furnace, and finally sintered at 1550ºC, 1600ºC or 1650ºC for 2 hours in air (Lindberg/Blue M furnace - model BF51634PCOMC, Ashville, NC). To evaluate the maximum load that can be carried by springs, compression tests were performed at room temperature in a mechanical testing machine (EMIC DL3000, PR, Brazil)[5], as shown in Fig. 1.

Figure 1

To avoid testing samples with macrovoids, only ceramic springs with green densities higher than 2.64 g/cm^3 were sintered and used in compression tests. For helical springs subjected to a longitudinal, uniaxial compressive force F, torsional and transverse shear stresses occur. The maximum torsional shear stress occurring at the inner part of treads can be calculated as follows[5]

$$\tau_{\max} = \frac{2F\left(12D^2 - 19dD - d^2\right)}{3\pi d^3 \left(D - 2d\right)} \tag{1}$$

where D is the mean spring diameter and d is the coil diameter. The transverse shear stress due to bending the wire is given as[6, 12]:

$$\tau_d = \frac{4F}{\pi d^2} \tag{2}$$

In the limit of $D/d >> 1$, the transverse shear stress can be neglected[12, 13]. In this study, Eq. (1) was used to determine the strength of ceramic springs.

Microstructural Analysis

The grain boundary was revealed by the thermal treatment of pre-polished sections of helical alumina springs at 1400^{o}C for 30 min. Images were obtained using a SSX-550 scanning electron microscope (Shimadzu, Japan) with carbon coated samples. Measurements of grain sizes were carried out by using the lineal intercept procedure according to ASTM E112 [17].

Weibull Failure Statistics

Failure of ceramics initiates from pre-existing flaws, and thus their strength depends on the size of the most critical flaw, which varies from one specimen to another. Therefore, the variation of position, orientation and size of a critical flaw causes scattering of strength in advanced ceramics. Therefore, a probability approach should be used in the design of ceramic springs.

The Weibull distribution[18, 19] is most widely used in the statistical analysis of strength and design of ceramics. The failure probability of a ceramic component due to volume flaws $P_{F,V}$ subjected to a multiaxial stress can be written as[20, 21]

$$P_{F,V}\left(\sigma^*, V_{eff}\right) = 1 - \exp\left[-\frac{V_{eff}}{V_0}\left(\frac{\sigma^*}{\sigma_0}\right)^m\right] \tag{3}$$

where σ^* is the reference stress ($\sigma^* = \tau_{max}$ for ceramic springs), V_{eff} can be described as the volume of a rod under tensile tests with the same stress distribution, V_0 is the unit volume containing the average number of cracks, σ is the uniaxial applied stress, m is the Weibull modulus which describes the scatter of strength, and σ_0 is the characteristic strength at which the failure probability is 63.2 % for a specimen with a volume of $V_{eff} = V_0$. The maximum likelihood estimators of σ_0 and m, which are obtained by maximizing its log-likelihood function, are given as[22]

$$\sigma_0 = \left\{\frac{1}{n}\sum_{i=1}^{n}\sigma_i^m\right\}^{1/m} \quad \text{and} \quad \frac{1}{m} = \frac{\sum_{i=1}^{n}\left[\sigma_i^m \ln(\sigma_i)\right]}{\sum_{i=1}^{n}\sigma_i^m} - \frac{1}{n}\sum_{i=1}^{n}\ln(\sigma_i) \tag{4}$$

Results & Discussion

During the sintering stage, ceramic springs were internally supported by an alumina cylinder to avoid distortion during shrinkage[5]. Typical springs after sintering are shown in Fig. 2. No cracks were observed after debinding and sintering and three sets of ceramic springs with well-defined shapes were obtained.

Figure 2

In Fig. 3, pictures of some broken alumina coil springs are shown. In Fig. 3(a), the crack plane is illustrated by using a dashed line and its angle is approximately equal to 45º. Nohut et al.[21]

investigated the angle of crack propagation in alumina ceramics by using tension-torsion tests. They reported that a normal stress criterion is in well agreement with experimental and numerical results and according to the normal stress criterion, the crack angle is equal to 45º when the specimen is loaded under pure torsion.

Figure 3

During the loading of ceramic springs, the effect of bending stress can be neglected compared to torsional stress; therefore crack propagates along an angle of 45º, as shown in Fig. 3(a). This result shows that, under a multiaxial stress, alumina springs fail following the normal stress criterion.
In Table 1, the relevant parameters are given for springs sintered at 1550°C, 1600°C and 1650°C, including the number of samples N, the mean values of wire diameter d and spring diameter D, and the Weibull parameters calculated by the maximum likelihood method[5].

Table 1

As Barbieri et al.[5] reported, the Weibull modulus m and the characteristic strength σ_0 increase as the increase of sintering temperature. In the calculation of fracture strength of ceramics springs by Eq. (1), the mean values of wire and spring diameters in Table 1 were used. In Fig. 4, the Weibull plot of strength of alumina springs sintered at different temperatures and the coefficient of determination R^2 values are given. Here, R^2 provides information about the goodness of fit of a model, which is a statistical measure of how well the regression line approximates real data. An R^2 of 1.0 indicates that the regression line perfectly fits the data. As R^2 decreases, the fitting quality of the regression line decreases. Comparison of R^2 values in Fig. 4 reveals that the Weibull distribution best fits the strength data of springs sintered at 1600°C. In Fig. 4(a-b), deviations (mostly at low strength values) from the Weibull line are observed for samples sintered at 1550°C and 1650°C.

Figure 4

Scanning electron microscopy images in Fig. 5 reveal the microstructure of alumina springs, which were obtained by secondary electrons.

Figure 5

The porosity, measured by Barbieri et al.[5] on the basis of the Archimedes´ method, and the average grain size of alumina springs are given in Table 2. Measurements of the average grain size were performed on scanning electron microscopy images by using the lineal intercept procedure[17].

Table 2

Alumina springs sintered at 1550°C have the highest porosity. As is well known, there are two main prerequisites for a Weibull distribution: (i) structure fails if one single flaw becomes critical (i.e., the weakest link hypothesis) and (ii) flaws do not interact. Thus, in most cases, the Weibull distribution can not be applied to porous materials[23, 24]. A group of pores as well as their interaction would affect the final fracture rather than only the largest one as the weakest-link model postulated[25]. The existence of a high ratio of pores (volume flaws) causes multiple flaw populations. Each individual flaw population has its typical size distribution and leads to a distribution with different Weibull parameters. As a result, the strength distribution resulting from different flaw populations will overlap, which cannot be modeled by one single tail of flaw size distribution. When there are multiple flaw populations, the failure probability for a given stress σ can be defined as[24]

$$P = 1 - \exp\left[-\left(\frac{\sigma}{\sigma_{0,1}} \right)^{m_1} - \left(\frac{\sigma}{\sigma_{0,2}} \right)^{m_2} \right] \tag{5}$$

where $\sigma_{0,1}$ and m_1 are the Weibull parameters of flaw type I (e.g., volume flaws) and $\sigma_{0,2}$ and m_2 are the Weibull parameters of flaw type II (e.g., surface flaws). Fig. 6 shows the Weibull plot of strength data of alumina springs sintered at 1550°C.

Figure 6

As shown in Fig. 6, the dashed line is the original Weibull plot and solid lines represent the Weibull plots with different flaw populations. It is evident that there are three types of Weibull distributions. Two kinks occur in the linear Weibull plot due to the multimodal flaw or the high porosity.

Figure 7

In Fig. 7, the pictures of crack propagation planes of broken alumina springs, sintered at 1550°C, are shown. Type-I represents the volume flaw and type-II represents the surface flaw. It is seen that volume flaws, surface flaws or both may be the main reason of failure and strength determinant for alumina springs sintered at 1550°C. As a result, it is not reliable to characterize the strength of these springs by a single flaw size distribution. This is the main reason for the deviation of strength distribution of alumina springs sintered at 1550°C from the Weibull line.

In Fig. 4(c), deviation from the Weibull line at low strength values is observed. As seen in Table 2, the average grain size increases as the increase of sintering temperature. There are numerous investigations which show the effect of the average grain size on the *R*-curve behavior (i.e., an increase of fracture resistance with the crack propagation) of alumina[27-31]. Wieninger et al.[32] measured crack resistance curves of three pure alumina ceramics with different grain sizes, in which flat crack resistance curves were reported for fine-grained alumina and steeply rising crack resistance curves for coarse grained alumina. This shows that as the grain size increases (> 2-3 μm), the *R*-curve effect increases. As a result, the *R*-curve effect can be observed in alumina springs sintered at 1650°C.

According to linear elastic fracture mechanics, the stress intensity factor increases with increasing applied load until a critical value of stress intensity factor K_I is reached, at which a crack is still in equilibrium and above which the unstable crack propagation takes place. Such a critical value is referred to as fracture toughness K_{IC}. When there is an *R*-curve effect, the crack growth resistance increases with the crack extension and the crack propagation behavior is no more characterized by a single value K_{IC} but with K_{IR}, which increases from K_{I0}, an onset value of crack growth (crack-tip toughness).

Owing to the existence of short (small) cracks in a material with the *R*-curve behavior, the unstable crack propagation occurs since the condition $K_I > K_{I0}$ is always fulfilled. As a result, there is no stable crack propagation. When a long crack exists in a material, as the condition $K_I = K_{I0}$ is satisfied, the crack starts to propagate in a stable manner. The unstable crack propagation occurs at a K_I value higher than K_{I0} after the stable crack growth. Therefore, it is obvious that the *R*-curve effect influences the strength of components with large cracks, but has no important effect on specimens with small defects[26]. The increasing crack growth resistance leads to an increase in the Weibull modulus m[24,26]. This explains the increase of the Weibull modulus with increasing sintering temperatures (see Table 1). It is concluded that, therefore, if a series of strength measurements are performed, specimens with large cracks (low strength) have a Weibull modulus higher than that with small cracks (high strength).

Figure 8

In Fig. 8, the Weibull plot of measured strengths of alumina springs sintered at 1650°C is given. The dashed lines indicate the original population and the solid line shows the effect of *R*-curve behavior.

For low strength data (failure due to large cracks), the Weibull modulus is higher than that for high strength data (failure due to small cracks). This shows the effect of *R*-curve behavior on strength distribution. This is the main reason for deviation of strength data of alumina springs sintered at 1650^{o}C from the Weibull distribution.

Conclusions

In this paper, the effect of sintering temperature on the microstructure and strength distribution of alumina coil springs was investigated. It is shown that the average grain size increases with the increase of sintering temperature. For the measured strengths of alumina springs sintered at 1550^{o}C and 1650 ^{o}C, deviations from the Weibull distribution were observed. Due to the high porosity in alumina springs sintered at 1550^{o}C, there are multimodal flaw populations (volume and surface flaws), which result in deviations of the strength distribution from the Weibull plot. According to grain size measurements, alumina springs sintered at 1650^{o}C have the largest average grain size. As the grain size increases, the *R*-curve effect appears which results in an increase of the Weibull modulus. As a conclusion, although the Weibull modulus is the highest (lowest scatter of strength) at the sintering temperature of 1650^{o}C, the strength data for alumina springs sintered at 1600^{o}C is best fitted by the Weibull distribution and the strength predicted by using the Weibull function is more reliable than that for springs sintered at 1550^{o}C and 1650^{o}C.

References

1. J. Rödel, A. B. N. Kounga, M. Weissenberg-Eibl, D. Koch, A. Bierwisch, W. Rossner, M. J.Hoffmann, R. Danzer and G. Schneider: *J. Eur. Ceram. Soc.,* 2009, **29**, (9), 1549-1560.
2. Y. Liang and S. P. Dutta: *Technovation*, 2001, **21**, (1), 61-65.
3. M. Matsui: *Ceram. Int.,*1993, **19**, (1), 9-16.
4. I. Krindges, R. Andreola, C. A. Perottoni and J. E. Zorzi: *Int. J. Appl. Ceram. Technol.*, 2008, **5**, (3), 243–248.
5. R. A. Barbieri, C. A. Perottoni, and J. E. Zorzi: *Int. J. Appl. Ceram. Tech.* doi: 10.1111/j.1744-7402.2011.00682.x.
6. J. B. Hamrock, B. O. Jacobson and S. R. Schmid: *Fundamentals of Machine Elements*, WCB/Mc-Graw-Hill, Singapore, 1999.
7. M. F. Ashby, *Materials Selection in Mechanical Design.* Butterworth-Heinemann, Oxford, UK, 2005.
8. J. Stockmann and W. Beckert, *Ceramic Spring Elements- From Design to Prototype.* Annual Report, p. 26, Fraunhofer IKTS, Germany, 2007.
9. W. Nakao, S. Mori, J. Nakamura, K. Takahashi and K. Ando: *J. Am. Ceram. Soc.,* 2006, **89**, (4), 1352-1357.
10. T. Hamilton, M. Gopal, E. Atchley and J. E. Smith Jr.: *J. Mater. Sci*., 2003, **38**, (15), 3331-3335.
11. C. Kaya and E. G. Butler: *Scr. Mater*., 2003, **48**, (4), 359-364.
12. S. Nohut and G. A. Schneider: *J. Eur. Ceram. Soc*. 2009, **29**, (6), 1013-1019.
13. S. Sato, K. Taguchi, R. Adachi and M. Nakatai: *Fatigue Fract. Eng. Mater. Struct.* 1996, **19**, (5), 529-537.
14. D. Rubesa and R. Danzer: *Forsch. Im Ingenierwes. Eng. Res. Bd.* 1995, **61**, (10), 249-254.
15. J. E. Zorzi, C. A. Perottoni, and J. A. H. da Jornada: *J. Mater. Sci.*, 2002, **37**, (9), 1801–1807.
16. J. E. Zorzi, C. A. Perottoni, and J. A. H. da Jornada: *Ind. Ceram*., 2003, **23**, (1), 47–49.
17. ASTM E 112 – *Standard Test Methods for Determining Average Grain Size*, p. 229-251.

18. W. Weibull: *Trans. Roy. Inst. Technol. 1949,* **27**, 5-50.

19. W. Weibull: *J. Appl. Mech*., 1951, **18**, (2), 293-297.

20. R. Danzer: *J. Eur. Ceram. Soc*. 1992, **10**, (6), 461-472.

21. S. Nohut, A. Usbeck, H. Özcoban, D. Krause and G. A. Schneider: *J. Eur. Ceram. Soc.* 2010, **30**, (16), 3339-3349.

22. H. L. Harter and A. H. Moore: *Technometrics* 1965, **7**, (4), 639-643.

23. C. Lu, R. Danzer and F. D. Fischer: *Phys. Rev. E* 2002, **65**, (6), 067102.

24. S. Nohut and C. Lu: *Ceram. Int*., 2012, doi:10.1016/j.ceramint.2012.02.093.

25. C. Lu, R. Danzer and F. D. Fischer: *J. Eur. Ceram. Soc.* 2004, **24**, (14), 3643–3651.

26. D. Munz and T. Fett: "*Ceramics: Mechanical Properties, Failure Behavior, Materials Selection"*, Springer Verlag, Berlin, Heidelberg, New York, 1999.

27. S. Nohut: *Comp. Mater. Sci*. 2011, **50,** (4), 1509-1519.

28. T. Tomaszewski, M. Boniecki and H. Weglarz: *J. Eur. Ceram. Soc.* 2000, **20**, (14-15), 2569-2574.

29. P. Chantikul, S. J. Bennison and B. R. Lawn: *J. Am. Ceram. Soc.*1990, **73**, (8), 2419-2427.

30. T. Fett, D. Munz, X. Dai and K. W. White: *Int. J. Fracture* 2000, **104**, (3), 375-385.

31. R. W. Steinbrech, A. Reich and W. Schaarwaecther: *J. Am. Ceram. Soc.*1990, **73**, (7), 2009-2015.

32. H. Wieninger, K. Kromp and R. F. Pabst: *J. Mater. Sci.* 1986, **21**, (2), 411-418.

Figure Captions

Figure 1 Compression testing machine and alumina spring under testing.

Figure 2 Alumina springs after the sintering stage.

Figure 3 Typical morphology of broken alumina springs. (a) The spring was broken into two parts and (b) the spring was broken into three parts.

Figure 4 Weibull plots of strength for alumina springs sintered at (a) 1550°C, (b) 1600°C, and (c) 1650°C.

Figure 5 Scanning electron microscopy images showing the microstructures of alumina springs sintered at (a) 1550^{o}C, (b) 1600^{o}C and (c) 1650^{o}C.

Figure 6 The Weibull plot of measured strengths of alumina springs sintered at 1550^{o}C. The dashed line indicates the original population and solid lines indicate different flaw populations.

Figure 7 Pictures of alumina springs which fractured due to volume flaws (type-I), surface flaws (type-II) and mixed flaws (type-I and type-II).

Figure 8 The Weibull strength plot of alumina springs sintered at 1650^{o}C. The dashed line indicates the original population and solid lines indicate the flaw population with an *R*-curve.

Tables

Table 1. Number and geometrical dimensions of spring samples at different sintering temperatures and parameters fitted by the Weibull distribution.

Sintering Temperature [°C]	N	d [mm]	D [mm]	m	σ_0 [MPa]
1550	41	4.06	23.15	1.88	39.03
1600	49	4.02	23.08	2.04	50.65
1650	47	4.04	22.91	2.35	52.08

Table 2. Porosity[5] and average grain size of alumina springs.

Sintering Temperature [°C]	Porosity, [vol. %]	Average Grain Size, [µm]
1550	6	1.5
1600	3.4	2.1
1650	2.5	5.4

Figure 1

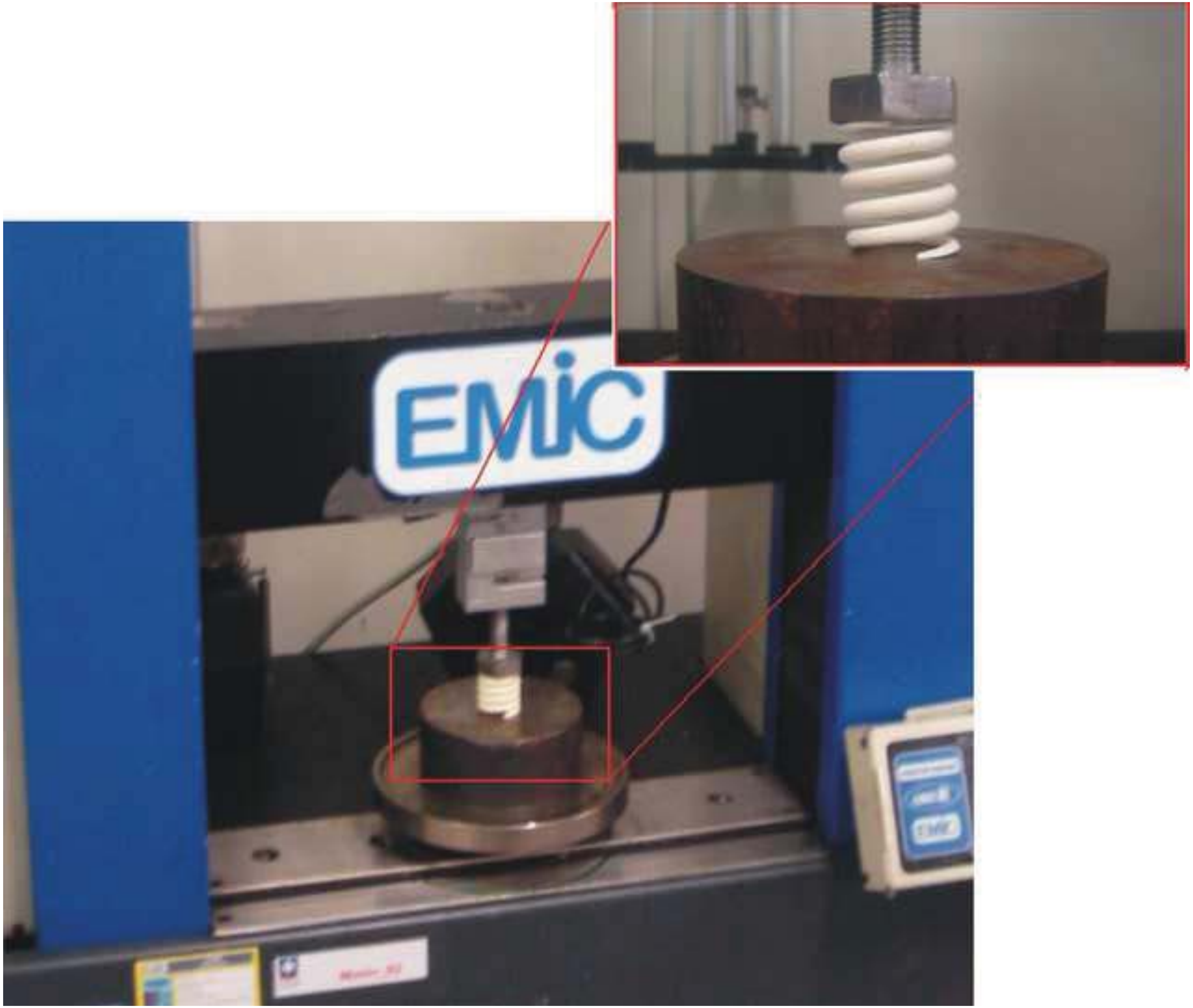

Figure 2

Figure 3

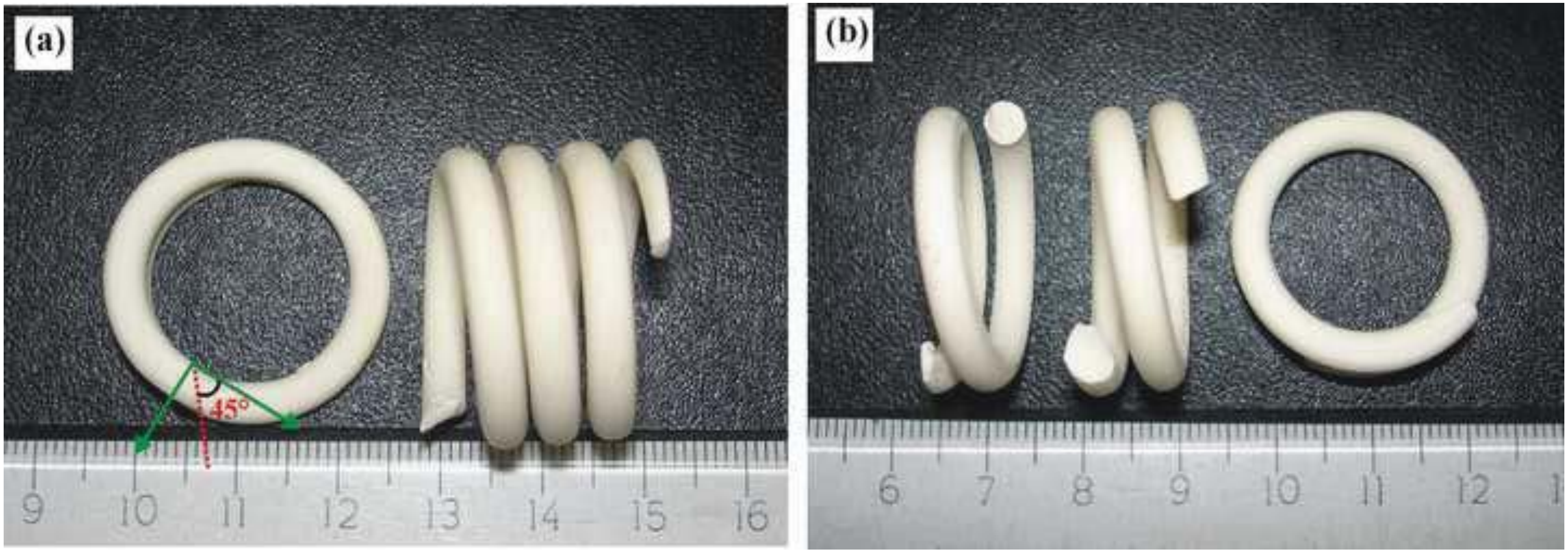

Figure 4
Click here to download high resolution image

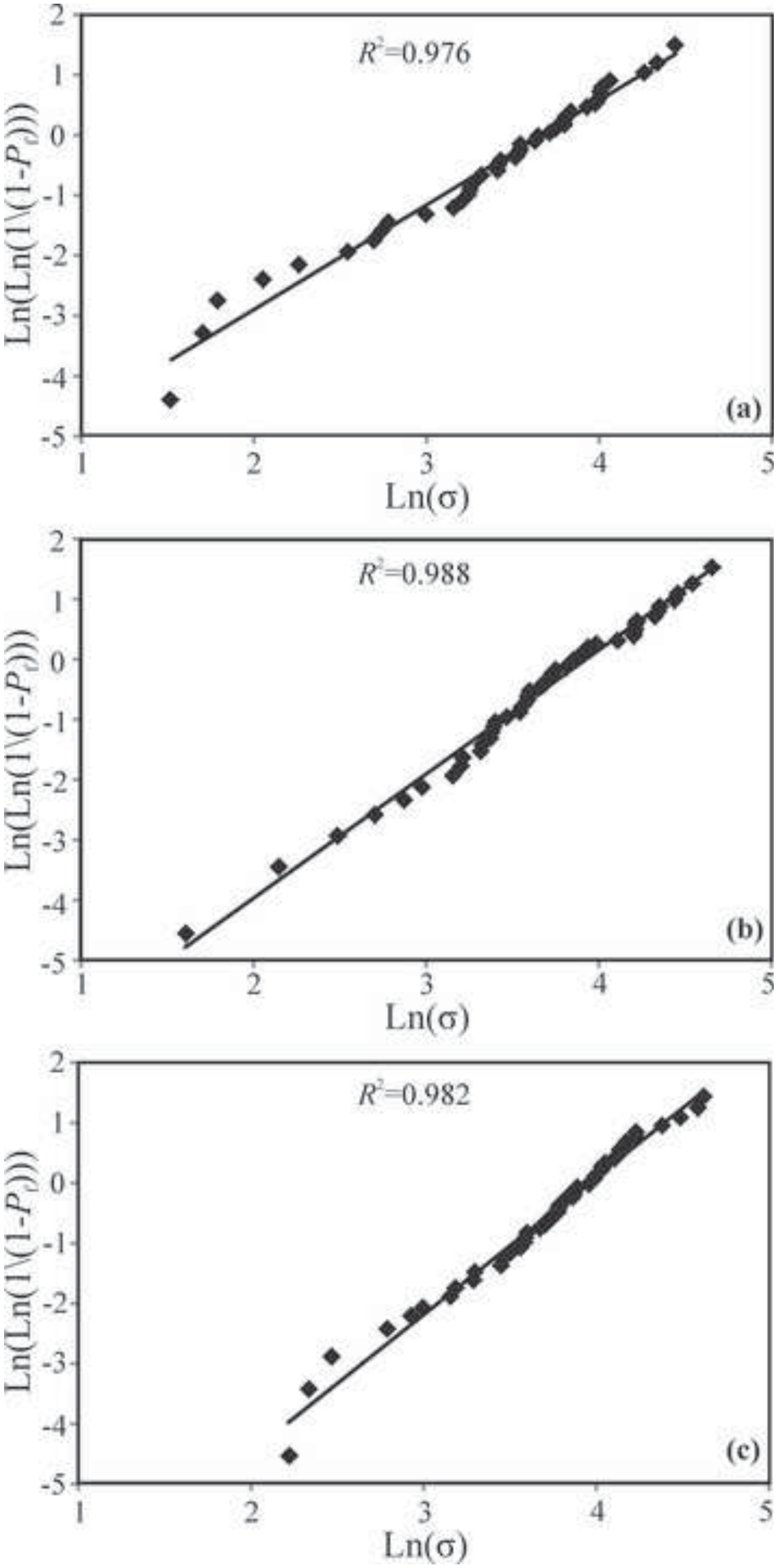

Figure 5
Click here to download high resolution image

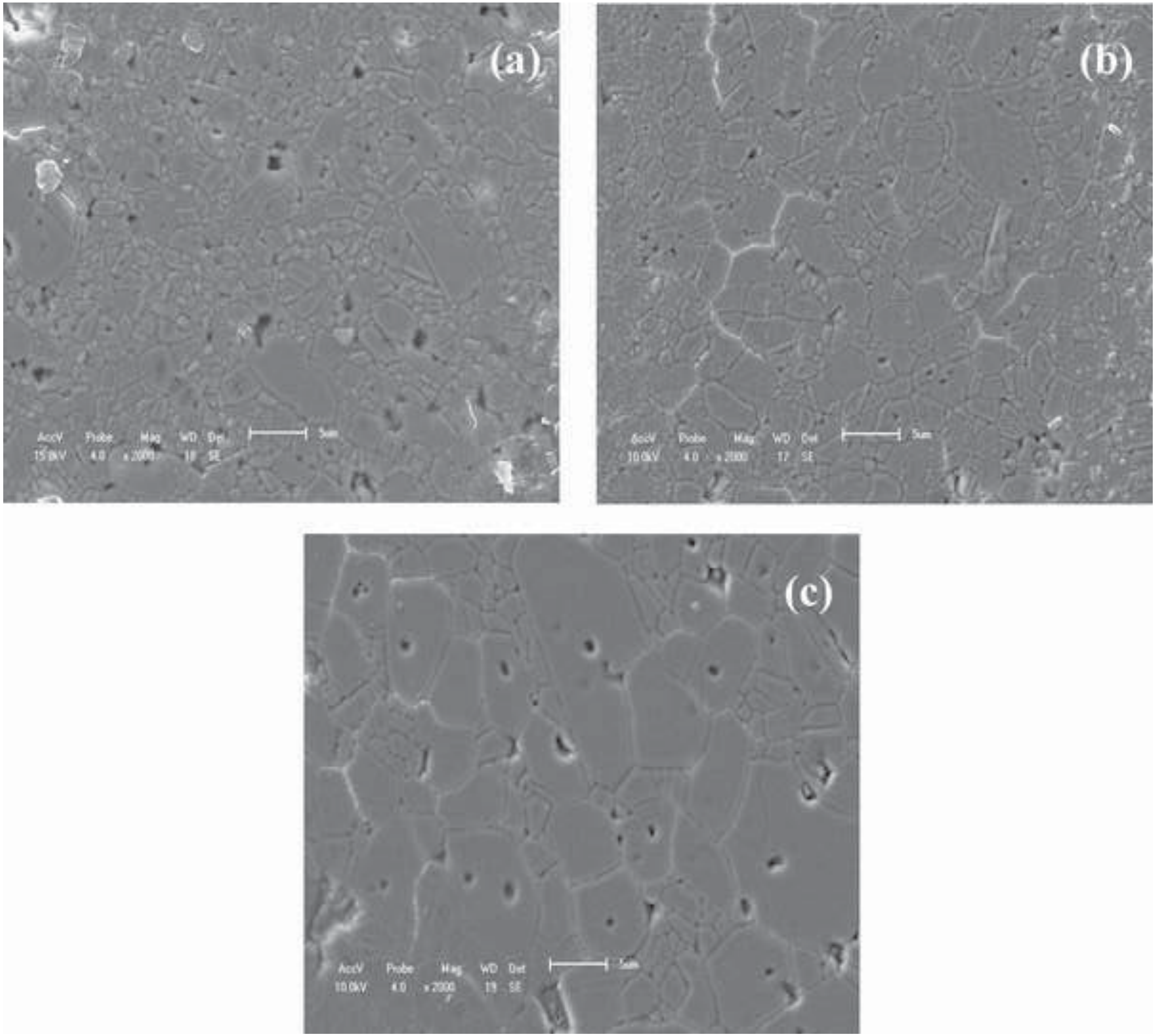

Figure 6

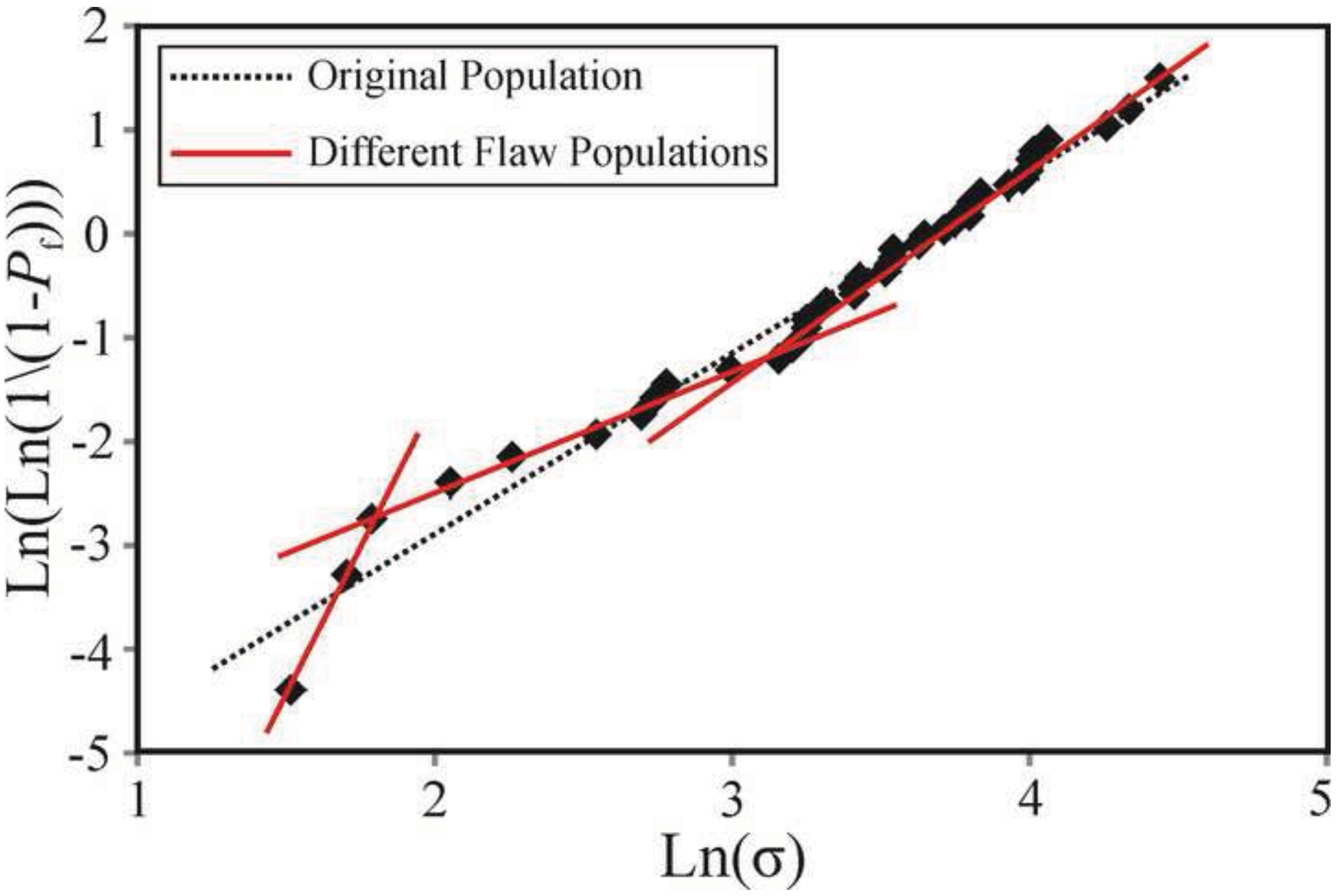
Original Population
Different Flaw Populations
Ln(Ln(1\(1-P_f)))
2
1
0
-1
-2
-3
-4
-5
1
2
3
4
5
Ln(σ)

Figure 7

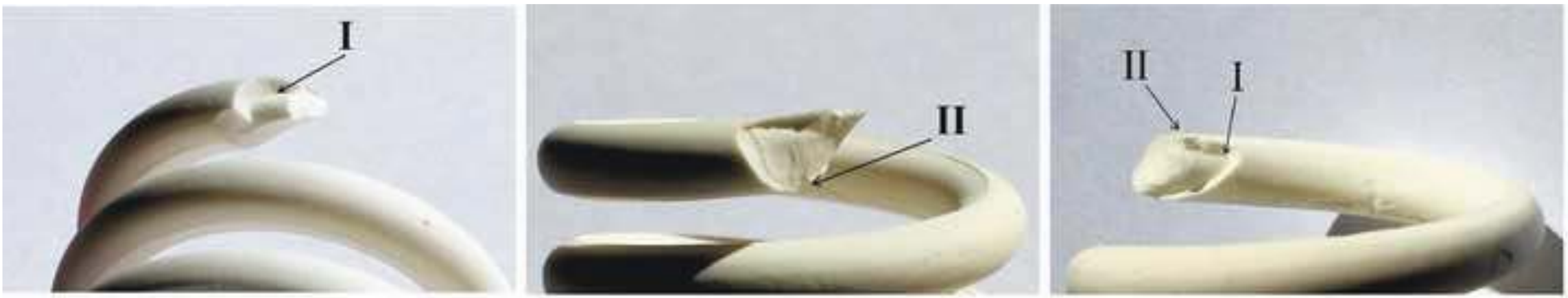

Figure 8

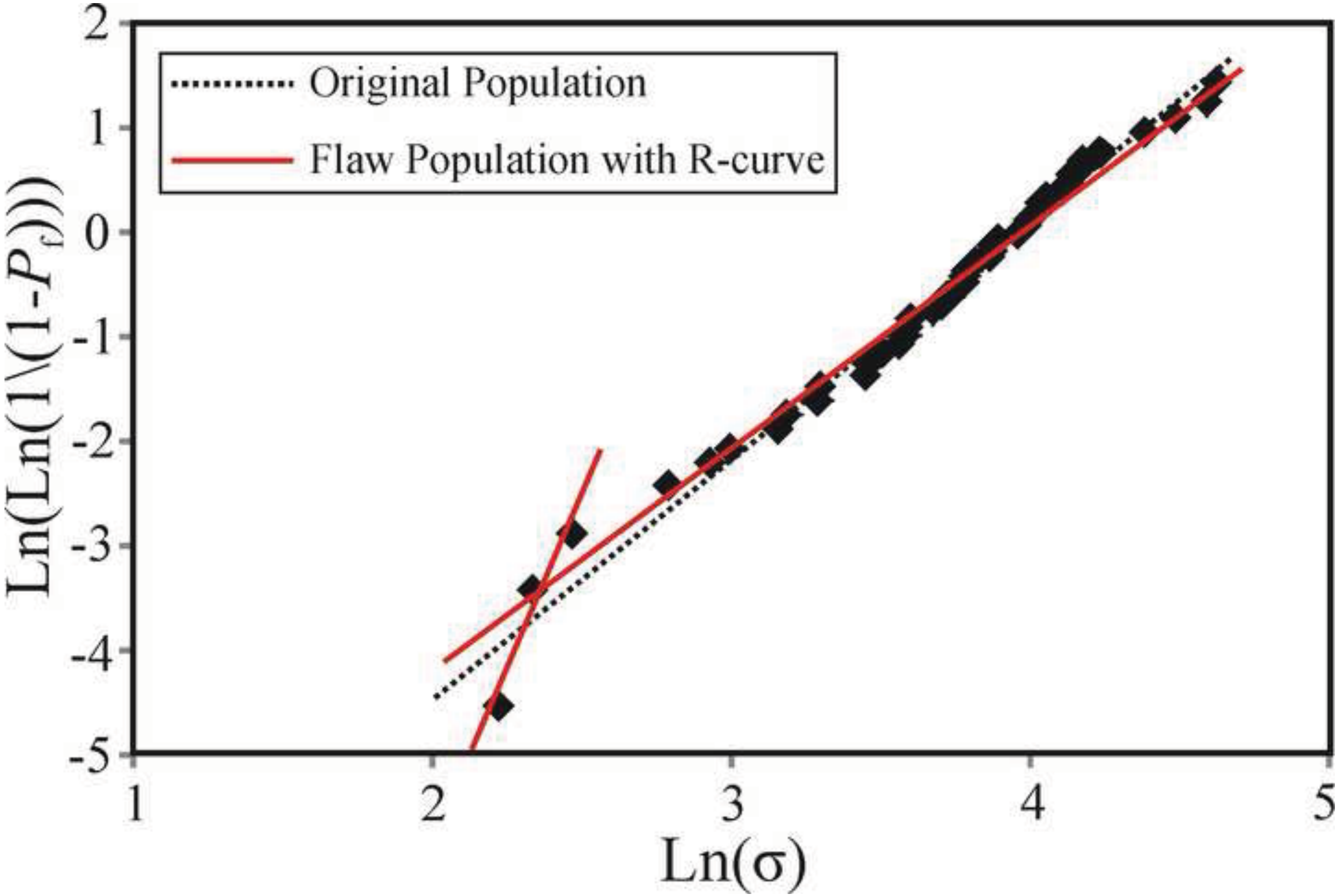
Original Population
Flaw Population with R-curve
Ln(Ln(1\(1-P_f)))
Ln(σ)
2
1
0
-1
-2
-3
-4
-5
1
2
3
4
5